Distributed Model Predictive Control Method for Spacecraft Formation Flying in a Leader-Follower Formation

PEDRO PEREIRA
NOVA School of Science and Technology (FCT-NOVA), NOVA University of Lisbon, Caparica 2829-516, Portugal

BRUNO J. GUERREIRO, Member, IEEE
NOVA School of Science and Technology (FCT-NOVA), NOVA University of Lisbon, Caparica 2829-516, Portugal

PEDRO LOURENÇO
GMV, Alameda dos Oceanos, no 115, 1990-392 Lisboa, Portugal

***Abstract*— This paper presents a Distributed Model Predictive Control (DMPC) algorithm for a scenario of spacecraft formation flying, namely spacecraft platooning in a leader-follower formation. This spacecraft formation application can be regarded as a cooperative system composed of several spacecraft with a common goal, for which a relative translational model is considered connecting the different agents. A distributed algorithm is proposed that solves a 1-hop optimization problem in order to estimate the optimal control action sequence, including also relevant constraints to protect and deal with the overall system. The algorithm is then analyzed in terms of uniqueness and convergence of the optimal control action. The proposed methods are validated with realistic simulation results, showing that all vehicles demonstrate reliable performance following a given trajectory or goal in a formation, while satisfying all the considered constraints.**

***Index Terms*— Distributed control, Predictive control, Satellite applications.**

I. Introduction

SPACE exploration has been a much discussed topic in recent years, due to the inherent curiosity of wanting to know more about how the Universe works, and possibly to take Human society outside of planet Earth. Within the immense complexity of planning and implementing a spacecraft for space navigation, some of the most important and difficult maneuvers to perform are the rendezvous and docking maneuvers [1], which make it possible to physically couple two spacecraft. These maneuvers are essential to transport goods or people from one spacecraft to another, for replenishment, assembly, maintenance, repair [2], space debris collection [3], [4] or even Earth observation. These tasks not only need to be performed successfully, but also incorporate autonomy into the systems, relying as little as possible in external human aid.

Over the years, different methods were considered for these proximity operations, but due to the computational limitations in space [5], there has been a focus on simpler and computationally lighter methods. Recently, with the development of more robust and capable embedded systems, more complex controllers are being considered for space operations, and among them is Model Predictive Control (MPC). MPC was initially considered for industrial applications, to control oil refineries, power plants and chemical processes [6], but in recent years the MPC has been vastly studied for flight control, docking and rendezvous maneuvers [7]–[9]. Using MPC techniques can bring important improvements to the overall performance of autonomous vehicles in general, and spacecraft in particular, at the cost of additional processing capabilities, which may be mitigated with carefully crafted methods. These techniques intrinsically enable the introduction of input and state constraints into the control law, while also being capable of accounting for future changes to references and constraints, according to the vehicle and mission requirements. For instance, in [10] and [11] robust MPC algorithms considering system constraints and disturbances are proposed for optimal time-varying attitude tracking control and for reentry vehicles, respectively.

Distributed techniques such as those proposed in this paper enable the effective use of MPC in communication restricted environments. One application of rendezvous maneuvers is spacecraft formation flying [12], [13], that consists in the cooperation of several spacecraft to achieve a specific objective, instead of sending a single, more expensive spacecraft. This topology allows to obtain a distributed model [14] between all the spacecraft, but sharing at the same time a common objective.

The proposed strategy is therefore a subset of the spacecraft formation flying scenario, where several follower spacecraft converge to the leader spacecraft orbit and establish a constant relative position between each other in a spacecraft platooning [15] formation. This is achieved using a Distributed Model Predictive Control (DMPC) strategy, where the system model consists of a coupled relative model between each spacecraft with a V-bar orbital station keeping trajectory. A spacecraft platooning system can have several uses, such as syn-

Manuscript received XXXXX 00, 0000; revised XXXXX 00, 0000; accepted XXXXX 00, 0000.
This work was partially funded by FCT projects REPLACE (PTDC/EEIAUT/32107/2017), which includes Lisboa 2020 and PIDDAC funds, CAPTURE (PTDC/EEIAUT/1732/2020), CTS (UIDB/00066/2020) and LARSYS (UIDB/50009/2020). *(Corresponding author: P. Pereira).*

Bruno J. Guerreiro is also with CTS-UNINOVA and with the Institute for Systems and Robotics (ISR), LARSYS, Lisbon, Portugal. (e-mails: pmp.pereira@campus.fct.unl.pt, bj.guerreiro@fct.unl.pt, and palourenco@gmv.com).

chronization, position correction, spacecraft retention on a specific orbit and also for Earth observation, where a group of spacecraft can orbit around the Earth and retrieve soil or meteorological information to be later analyzed and compared.

Given the interaction needed between the agents for a platooning scenario, it becomes important to reinforce the cooperative component of this type of maneuver. There are several distributed approaches that can be used, but consensus based algorithms have proven over time to be reliable tools for dealing with multiple agents systems [16], [17]. Therefore, the 1-hop local optimization algorithm, presented in [18], is considered as the basis for formulating the new distributed algorithm that will be proposed. The concept of 1-hop refers to the interaction of an agent with all its neighbors that are directly interconnected, that is, to a first-order neighborhood. Furthermore, a variety of network topologies are presented specifically for the platooning and leader-follower formation.

Some MPC distributed approaches for a multi-agent system include [15] where the platoon problem is studied for a group of heterogeneous vehicles that follow a unidirectional network topology with leader-follower formation and in [19] where, in a simulation environment, the distributed MPC is compared with the centralized one for a group of UAVs in order to arrive at a given flight formation, using a non-linear kinematic model and allowing the exchange of information, such as its position, to avoid collisions between agents. For the spacecraft formation flying scenario, in [20] it is studied the main concepts of cooperation, formation flying, fault recovery and communication delays in a MPC-based design, and comparing its performance to other configurations, such as the centralized and decentralized models, where the distributed outperformed in terms of minimizing the control effort and the necessary compensation for failures.

A preliminary version of this work [21] focuses in two different cooperative spacecraft formation flying strategies: spacecraft platooning and on-orbit spacecraft servicing. For this spacecraft platooning system, the same scenario is considered, where several follower spacecraft converge to the leader spacecraft orbit and establish a constant relative position between each other, but with the condition that the topology must be unidirectional and in series, which restricts the communication and interaction capacity of the spacecrafts involved. Therefore, the problem previously presented in [21] is expanded, by proposing a second strategy that allows different network topologies to be considered, through the use of Graph Theory and Distributed MPC techniques. Also, instead of considering all the relative states of every spacecraft, in this case it is considered a neighborhood error for each agent, which results in less mathematical calculation to be made. And finally, the 1-hop interactive local optimization algorithm proposed, results in a more trustworthy solution, when compared to the simple convex step distributed algorithm used in [21], for this cooperative scenario. In this 1-hop optimization algorithm, each agent uses its neighborhood in order to converge to a optimal solution, by incorporating a neighborhood dynamics error instead of considering the state of every spacecraft involved. In addition to that, it is shown that the proposed distributed algorithm and optimization problem follows the conditions of convergence and uniqueness respectively. The proposed method is also validated through simulation results, showing reliable performance for several network topologies while satisfying all the considered constraints.

The remainder of this paper is structured as follows. Section II contains a brief background of spacecraft formation flying dynamics. Section III outlines the MPC design for the spacecraft platooning system, including the system model, the distributed optimal control problem, the distributed algorithm and the constraints. Simulation results for the proposed strategy are presented in Section IV. Conclusions and future work are discussed in Section V.

II. Spacecraft Relative Motion

This Section introduces the general notation and mathematical background for spacecraft formation flying starting with the main coordinate reference frames, moving on to the relative translational motion for spacecraft and finally the Clohessy-Wiltshire (CW) equation.

Towards this end, we define three coordinate reference frames. The Earth Centered Inertial (ECI) frame, denoted as $\mathcal{F}^i : \{O_i, \hat{\mathbf{i}}_i, \hat{\mathbf{j}}_i, \hat{\mathbf{k}}_i\}$, has its origin located in the center of the Earth. The $\hat{\mathbf{i}}_i$ axis is directed towards the vernal equinox, $\hat{\mathbf{k}}_i$ is directed along the rotation axis of the Earth towards the celestial North Pole and $\hat{\mathbf{j}}_i$ completes the right-handed orthogonal frame. The Spacecraft Orbit reference frame, denoted as $\mathcal{F}^{so} : \{O_s, \hat{\mathbf{i}}_{so}, \hat{\mathbf{j}}_{so}, \hat{\mathbf{k}}_{so}\}$, is a Local-Vertical-Local-Horizontal (LVLH) frame with its origin located in the center of mass of the spacecraft. The $\hat{\mathbf{i}}_{so}$ axis is directed along the radius vector ${}^i\mathbf{r}_s \in \mathbb{R}^3$ in the $\mathcal{F}^i$ frame, that goes from the center of the Earth to the spacecraft, $\hat{\mathbf{k}}_{so}$ is pointing in the orbit normal direction, parallel to the orbit momentum vector and $\hat{\mathbf{j}}_{so}$ completes the right-handed orthogonal frame. For our application, s denotes the spacecraft in question, e.g. $s = l$ for the leader and $s = f$ for the follower. Finally, the Spacecraft Body Reference frame, denoted as $\mathcal{F}^{sb} : \{O_s, \hat{\mathbf{i}}_{sb}, \hat{\mathbf{j}}_{sb}, \hat{\mathbf{k}}_{sb}\}$, has its origin located in the center of mass of the spacecraft, with the basis vectors aligned with the principal body axes.

A. Relative Translational Motion

Consider a leader-follower spacecraft formation, composed by a single passive leader spacecraft and more than one active follower spacecraft, where the position vector of the leader and the follower expressed in $\mathcal{F}^i$ are defined respectively as ${}^i\mathbf{r}_l$ and ${}^i\mathbf{r}_f$, as seen in Fig. 1, and that the leader spacecraft is in a circular orbit about the Earth.

The relative position vector between the leader and the follower can therefore be expressed in the orbital frame

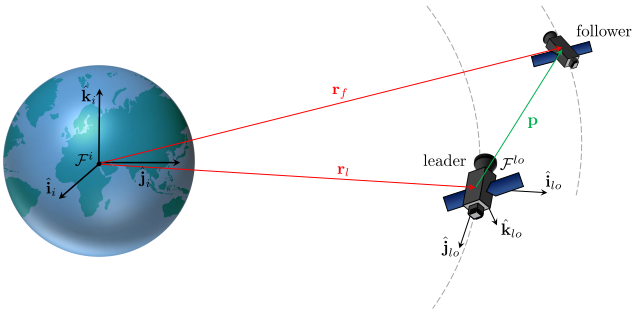

Fig. 1: Reference coordinate frames in a leader-follower formation

$\mathcal{F}^{lo}$ as

$$\mathbf{p} = \mathbf{R}_i^{lo}({}^i\mathbf{r}_f - {}^i\mathbf{r}_l) = \begin{bmatrix} x & y & z \end{bmatrix}^T \tag{1}$$

and the relative velocity as $\mathbf{v} = \dot{\mathbf{p}}$, where $\mathbf{R}_i^{lo} \in \mathcal{SO}(3)$ is the rotation matrix from $\mathcal{F}^i$ to the $\mathcal{F}^{lo}$ frame and $\mathcal{SO}(3)$ is the 3D rotation group defined as $\mathcal{SO}(3) = \{\mathbf{R} \in \mathbb{R}^{3\times3} : \mathbf{R}^T\mathbf{R} = \mathbf{R}\mathbf{R}^T = \mathbf{I}_3, \quad \det(\mathbf{R}) = 1\}$ with $\mathbf{I}_3 \in \mathbb{R}^{3\times3}$ as the identity matrix.

Assuming that the distance between the spacecraft is much smaller than the distance to the center of the Earth, with a maximum relative position into the tens of kilometers [22], the nonlinear relative translational dynamics can be derived for circular orbits and linearized around the origin of $\mathcal{F}^{lo}$ to get the well known CW equation [23]. Following the CW assumptions, it is considered that all the actuated follower spacecraft can keep connected with the passive leader. As such, applying the Taylor series expansion to nonlinear relative translational dynamics [22, Appendix A] yields

$$\begin{cases} \ddot{x} - 3n^2x - 2n\dot{y} = u_x \\ \ddot{y} + 2n\dot{x} = u_y \\ \ddot{z} + n^2z = u_z \end{cases}, \tag{2}$$

where n is the orbital rate given by $n = \sqrt{\frac{\mu}{\|{}^i\mathbf{r}_l\|^3}}$ and the follower control acceleration is defined as

$$\mathbf{u} = \frac{1}{m_f}\mathbf{f}_f = \begin{bmatrix} u_x & u_y & u_z \end{bmatrix}^T. \tag{3}$$

III. Distributed MPC for Spacecraft Platooning

Consider a system composed of λ follower spacecraft with masses m_i, $i = 1, 2, ..., \lambda$, such that each spacecraft f wants to follow spacecraft $f-1$ in a V-bar station keeping trajectory [24] with constant relative position and is followed by spacecraft $f+1$ the same way. Consider the spacecraft 0 as the leader of the spacecraft formation.

A. System Model

For the distributed strategy, it is assumed that the follower agents are able to exchange their information via a communication topology restricted by a connected directed graph $\mathcal{G} = (\mathcal{N}, \mathcal{I})$ where $\mathcal{N} = \{1, ..., \lambda\}$ is the set of agents representing the vertices of the graph and $\mathcal{I} \subseteq \mathcal{N} \times \mathcal{N}$ is the set of edges that connect the vertices/nodes. It is further assumed that all the follower agents are interconnected to the leader, in order to have a common orbital frame, in this case the $\mathcal{F}^{lo}$ frame. Some relevant examples of network topologies for the platoon scenario in a leader-follower formation are represented in Fig. 2.

The CW equation, expressed in (2), for a follower f relative to the leader can be rewritten as

$$\dot{\mathbf{x}}_f(t) = \mathbf{A}_c\mathbf{x}_f(t) + \mathbf{B}_c\mathbf{u}_f(t) \tag{4}$$

where $\mathbf{x}_f = \begin{bmatrix} \mathbf{p}_f^T & \mathbf{v}_f^T \end{bmatrix}^T \in \mathbb{R}^6$ is the state vector, $\mathbf{p}_f \in \mathbb{R}^3$ is the relative position expressed in $\mathcal{F}^{lo}$, $\mathbf{v}_f \in \mathbb{R}^3$ is the relative velocity expressed in $\mathcal{F}^{lo}$, t is the continuous time variable and

$$\mathbf{A}_c = \begin{bmatrix} 0 & 0 & 0 & 1 & 0 & 0 \\ 0 & 0 & 0 & 0 & 1 & 0 \\ 0 & 0 & 0 & 0 & 0 & 1 \\ 3n^2 & 0 & 0 & 0 & 2n & 0 \\ 0 & 0 & 0 & -2n & 0 & 0 \\ 0 & 0 & -n^2 & 0 & 0 & 0 \end{bmatrix}, \quad \mathbf{B}_c = \begin{bmatrix} \mathbf{0}_{3\times3} \\ \mathbf{I}_3 \end{bmatrix} \tag{5}$$

with n as the orbital rate of the leader. A Zero-Order Hold (ZOH) discretization is performed for expression (4), as suggested in [25], which yields

$$\mathbf{x}_f(k+1) = \mathbf{A}\mathbf{x}_f(k) + \mathbf{B}\mathbf{u}_f(k) \tag{6}$$

where

$$\mathbf{A} = e^{\mathbf{A}_c T_s}, \quad \mathbf{B} = \mathbf{B}_c \int_{t=0}^{T_s} e^{\mathbf{A}_c t} dt \tag{7}$$

with k as the discrete time variable and T_s as the sampling time. Expression (6) can be also written as

$$\mathbf{x}_f^+ = \mathbf{A}\mathbf{x}_f + \mathbf{B}\mathbf{u}_f. \tag{8}$$

In order to study the synchronization problem it is defined a neighborhood error for each agent f, given by

$$\mathcal{E}_f = \sum_{i\in\mathcal{N}_f} (\mathbf{x}_f - \mathbf{x}_i) + g^f\mathbf{x}_f \tag{9}$$

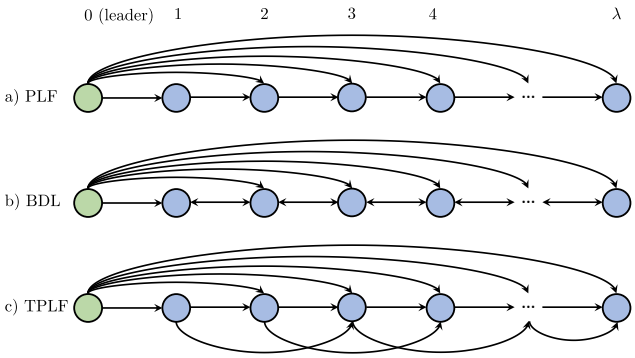

Fig. 2: Examples of network topologies for the platoon scenario in a leader-follower formation, adapted from [15]. a) predecessor-leader following (PLF), b) bidirectional with leader (BDL), c) two-predecessor-leader following (TPLF)

and from expressions (8) and (9) the error dynamics can be defined by

$$\mathcal{E}_f^+ = \mathbf{A}\mathcal{E}_f + (g^f + d^f)\mathbf{B}\mathbf{u}_f - \mathbf{B}\sum_{i\in\mathcal{N}_f}\mathbf{u}_i \tag{10}$$

where $\mathcal{N}_f \subset \mathcal{N}$ is the set of neighbors of agent f, $d^f = \|\mathcal{N}_f\|$ is the degree of agent f and $g^f = 1$ if the agent f is connected to the leader or $g^f = 0$ if not.

The graph $\mathcal{G}$ is defined by an augmented Laplacian matrix $\bar{\mathbf{L}} \in \mathbb{R}^{\lambda\times\lambda}$ given by

$$\bar{\mathbf{L}} = \mathbf{G} + \mathbf{D} - \mathbf{A}_d \tag{11}$$

where $\mathbf{G} = \text{diag}(g^1, \cdots, g^\lambda) \in \mathbb{R}^{\lambda\times\lambda}$ is the matrix that represents the connection to the leader and $\mathbf{D} = \text{diag}(d^1, \cdots, d^\lambda) \in \mathbb{R}^{\lambda\times\lambda}$ is the degree matrix. There is still the adjacency matrix $\mathbf{A}_d = [a_{ij}] \in \mathbb{R}^{\lambda\times\lambda}$ which describes the directional communication between the follower agents, with each entry expressed as

$$a_{ij} = \begin{cases} 1, & \text{if } i \neq i \text{ and } \{j,i\} \in \mathcal{I} \\ 0, & \text{else} \end{cases} \tag{12}$$

where $\{j,i\} \in \mathcal{I}$ means that there is a directional edge from node j to node i ($j \to i$). In order to obtain $\bar{\mathbf{L}}$ and its respective matrices, one can observe the communication relationship between each agent in Fig 2.

B. Distributed Model Predictive Control (DMPC)

For each agent $f \in \mathcal{N}$ it is intended to determine the optimal control sequence $\mathbf{U}_f^*$ that solves the 1-hop local optimization problem

$$\begin{aligned} \min_{\mathbf{U}_f} \quad & \mathbf{V}_f(\mathbf{U}_f; \mathcal{E}_f, \mathbf{U}_{-f_1}) \\ \text{s.t.} \quad & \text{expression (10)}, \quad \forall_{k=0,\ldots,N-1}, \\ & \mathcal{E}_f \in \mathcal{X}_f, \quad \forall_{k=0,\ldots,N}, \\ & \mathbf{u}_f \in \mathcal{U}_f, \quad \forall_{k=0,\ldots,N-1} \end{aligned} \tag{13}$$

such that

$$\mathbf{V}_f(\mathbf{U}_f; \mathcal{E}_f, \mathbf{U}_{-f_1}) = \alpha_f \left[\sum_{k=0}^{N-1}\left(\hat{\mathcal{E}}_f^T\mathbf{Q}\hat{\mathcal{E}}_f + \mathbf{u}_f^T\mathbf{W}\mathbf{u}_f\right) + \hat{\mathcal{E}}_f^T(N)\mathbf{P}\hat{\mathcal{E}}_f(N)\right], \tag{14}$$

$$\hat{\mathcal{E}}_f = \mathcal{E}_f - (g^f + d^f)\mathcal{E}_d \tag{15}$$

and where N is the prediction horizon, α is the cost function weight always different from zero, $\mathcal{E}_d \in \mathbb{R}^6$ is the desired tracking error, $\mathbf{P} \in \mathbb{R}^{6\times6}$ the final output error penalty, $\mathbf{Q} \in \mathbb{R}^{6\times6}$ the output error penalty and $\mathbf{W} \in \mathbb{R}^{3\times3}$ the control action penalty, all positive definite. There is also the set of linear constraints for state variables $\mathcal{X}$ and the set of linear constraints for control variables $\mathcal{U}$. Error $\mathcal{E}_d$, in expression (15), is also multiplied by $(g^f + d^f)$, in order to have a desired error that is proportional to the number of neighbors of the agent, leader included, which is an approach different from the one proposed in [18] in order to achieve a better separation between agents. For the optimization problem, $\mathbf{U}_f$ is considered as the optimization variable for the local problem, but the solution depends on the local error $\mathcal{E}_f$ and on the sequence $\mathbf{U}_{-f_1}$ which is associated with the 1-hop neighbors of f. In addition to that, $\mathcal{E}_d$ can be declared as a constant value that the vehicles have to maintain throughout their mission or create a variable error function that takes into account the proximity with the rendezvous target, and decreases the inter-vehicle distance as the formation approaches the target.

Converting to the batch format, the model dynamics of each agent $f \in \mathcal{N}$ (10) can be rewritten as

$$\mathcal{E}_f^{+:N} = \mathcal{A}\mathcal{E}_f + (g^f + d^f)\mathcal{B}\mathbf{U}_f - \mathcal{B}\sum_{i\in\mathcal{N}_f}\mathbf{U}_i \tag{16}$$

with

$$\mathcal{A} = \begin{bmatrix} \mathbf{A} \\ \mathbf{A}^2 \\ \vdots \\ \mathbf{A}^N \end{bmatrix}, \quad \mathcal{B} = \begin{bmatrix} \mathbf{B} & \mathbf{0} & \cdots & \mathbf{0} \\ \mathbf{AB} & \mathbf{0} & \cdots & \mathbf{0} \\ \vdots & \vdots & \ddots & \vdots \\ \mathbf{A}^{N-1}\mathbf{B} & \mathbf{A}^{N-2}\mathbf{B} & \cdots & \mathbf{B} \end{bmatrix} \tag{17}$$

such as the cost function, which yields

$$\begin{aligned} &\mathbf{V}_f(\mathbf{U}_f; \mathcal{E}_f, \mathbf{U}_{-f_1}) = \mathbf{U}_f^T\mathcal{W}\mathbf{U}_f + \\ &\left[\mathcal{E}_f^{+:N} - (g^f + d^f)\bar{\mathcal{E}}_d\right]^T \mathcal{Q}\left[\mathcal{E}_f^{+:N} - (g^f + d^f)\bar{\mathcal{E}}_d\right] + \\ &\left[\mathcal{E}_f - (g^f + d^f)\mathcal{E}_d\right]^T \alpha_f\mathbf{Q}\left[\mathcal{E}_f - (g^f + d^f)\mathcal{E}_d\right] \end{aligned} \tag{18}$$

where

- $\mathcal{Q} = \alpha_f\,\text{diag}(\mathbf{Q}, \cdots, \mathbf{Q}, \mathbf{P}) \in \mathbb{R}^{6N\times6N}$;
- $\mathcal{W} = \alpha_f\,\text{diag}(\mathbf{W}, \mathbf{W}, \cdots, \mathbf{W}) \in \mathbb{R}^{3N\times3N}$;
- $\bar{\mathcal{E}}_d = \begin{bmatrix}\mathcal{E}_d^T & \cdots & \mathcal{E}_d^T\end{bmatrix}^T \in \mathbb{R}^{6N}$.

By incorporating the expression (16) into (18) the cost function can be rewritten as

$$\mathbf{V}_f(\mathbf{U}_f; \mathcal{E}_f, \mathbf{U}_{-f_1}) = \mathbf{U}_f^T\mathbf{S}_f\mathbf{U}_f + 2\mathbf{s}_f^T\mathbf{U}_f + c_f \tag{19}$$

with

$$\begin{aligned} &\mathbf{S}_f = (g^f + d^f)^2\mathcal{B}^T\mathcal{Q}\mathcal{B} + \mathcal{W}, \\ &\mathbf{s}_f = (g^f + d^f)\mathcal{B}^T\mathcal{Q}\left[\mathcal{A}\mathcal{E}_f - \mathcal{B}\sum_{i\in\mathcal{N}_f}\mathbf{U}_i - (g^f + d^f)\bar{\mathcal{E}}_d\right], \\ &c_f = 2\left[\mathcal{B}\sum_{i\in\mathcal{N}_f}\mathbf{U}_i + (g^f + d^f)\bar{\mathcal{E}}_d\right]^T \mathcal{Q}\mathcal{B}\sum_{i\in\mathcal{N}_f}\mathbf{U}_i + \\ &\quad - 2\left[\mathcal{B}\sum_{i\in\mathcal{N}_f}\mathbf{U}_i + (g^f + d^f)\bar{\mathcal{E}}_d\right]^T \mathcal{Q}\mathcal{A}\mathcal{E}_f + \\ &\quad \mathcal{E}_f^T[\mathcal{A}^T\mathcal{Q}\mathcal{A} + \alpha_f\mathbf{Q}]\mathcal{E}_f - 2\alpha_f(g^f + d^f)\mathcal{E}_f^T\mathbf{Q}\mathcal{E}_d + \\ &\quad (g^f + d^f)^2\alpha_f\mathcal{E}_d^T\mathbf{Q}\mathcal{E}_d + (g^f + d^f)^2\bar{\mathcal{E}}_d^T\mathbf{Q}\bar{\mathcal{E}}_d. \end{aligned}$$

Considering the first-order optimality condition for vehicle f given by

$$\nabla_{\mathbf{U}_f}\,\mathbf{V}_f\left(\mathbf{U}_f; \mathcal{E}_f, \mathbf{U}_{-f_1}\right)\big|_{\mathbf{U}_f = \mathbf{U}_f^*} = \mathbf{0} \tag{20}$$

the result is

$$\mathbf{S}_f\mathbf{U}_f^* - (g^f + d^f)(\mathcal{B}^T\mathcal{Q}\mathcal{B})\sum_{i\in\mathcal{N}_f}\mathbf{U}_i + (g^f + d^f)^2(\mathcal{B}^T\mathcal{Q})\bar{\mathcal{E}}_d - (g^f + d^f)(\mathcal{B}^T\mathcal{Q}\mathcal{A})\mathcal{E}_f = \mathbf{0}. \tag{21}$$

Considering all agents, the optimal control sequence $\mathbf{U}$ can be found by solving the unconstrained optimization problem given by

$$\min_{\mathbf{U}} \quad \mathbf{V}(\mathbf{U};\mathcal{E}) = \sum_{f\in\mathcal{N}}\mathbf{V}_f(\mathbf{U}_f;\mathcal{E}_f,\mathbf{U}_{-f_1}) \tag{22}$$

for which the first-order optimality condition, obtained combining expression (21) for each f, is given by

$$\mathbf{S}\mathbf{U}^* + \left[(\mathbf{G}+\mathbf{D})\otimes\mathcal{B}^T\mathcal{Q}\mathcal{A}\right]\mathcal{E} - \left[(\mathbf{G}+\mathbf{D})^2\otimes\mathcal{B}^T\mathcal{Q}\right](\bar{\mathcal{E}}_d)_{\times\lambda} = \mathbf{0} \tag{23}$$

where

$$\mathbf{S} = (\mathbf{G}+\mathbf{D})\bar{\mathbf{L}}\otimes\mathcal{B}^T\mathcal{Q}\mathcal{B} + \mathbf{I}_\lambda\otimes\mathcal{W}. \tag{24}$$

The combined optimal control action sequence is then

$$\mathbf{U}^* = -\mathbf{K}\mathcal{E} + \mathbf{K}_d(\bar{\mathcal{E}}_d)_{\times\lambda} \tag{25}$$

with

$$\mathbf{K} = \mathbf{S}^{-1}\left((\mathbf{G}+\mathbf{D})\otimes\mathcal{B}^T\mathcal{Q}\mathcal{A}\right), \tag{26}$$

$$\mathbf{K}_d = \mathbf{S}^{-1}\left((\mathbf{G}+\mathbf{D})^2\otimes\mathcal{B}^T\mathcal{Q}\right). \tag{27}$$

The operator $\otimes$ refers to the Kronecker product, which is an operation on two matrices of arbitrary size resulting in a block matrix, such that, if $\mathbf{N}\in\mathbb{R}^{n_1\times n_2}$ and $\mathbf{H}\in\mathbb{R}^{n_3\times n_4}$, then $\mathbf{N}\otimes\mathbf{H}\in\mathbb{R}^{(n_1n_3)\times(n_2n_4)}$. In order to study the uniqueness of $\mathbf{U}^*$, consider the following Lemma 1.

LEMMA 1. *The augmented Laplacian matrix, given by $\bar{\boldsymbol{L}} = \boldsymbol{G}+\boldsymbol{D}-\boldsymbol{A}_d = \boldsymbol{G}+\boldsymbol{L}$, is positive definite.*

Proof:
First, it is necessary to prove that the Laplacian matrix $\mathbf{L} = \mathbf{D}-\mathbf{A}_d$ is positive semi-definite. For any $\mathbf{e}\in\mathbb{R}^{n_0}$, the Laplacian matrix is in quadratic format, more specifically

$$\mathbf{e}^T\mathbf{L}\mathbf{e} = \mathbf{e}^T\left(\sum_{(i,j)\in\mathcal{I}}\mathbf{L}_{i,j}\right)\mathbf{e}\sum_{(i,j)\in\mathcal{I}}\mathbf{e}^T\mathbf{L}_{i,j}\mathbf{e} = \sum_{(i,j)\in\mathcal{I}}(\mathbf{e}_i-\mathbf{e}_j)^2 \geq 0 \tag{28}$$

therefore $\mathbf{L}$ is positive semi-definite, or $\mathbf{L}\succeq 0$. In addition to that, since all the follower agents are interconnected to the leader, the matrix $\mathbf{G}$ will always have positive elements on its diagonal, making $\mathbf{G}$ positive definite. Therefore, since $\mathbf{L}$ is positive semi-definite the expression $\mathbf{G}+\mathbf{L}$ is positive definite, or $\bar{\mathbf{L}}\succ 0$. ■

PROPOSITION 2. *The optimal control action sequence $\boldsymbol{U}^*$ is a unique global minimum of (22).*

Proof:
If the expression $\mathbf{S}$ is invertible, then $\mathbf{U}^*$ exists and is unique. The proof will follow by showing that $\mathbf{S}$ is positive definite, and, therefore, invertible.

Let $\boldsymbol{\upsilon}$ and φ be an arbitrary eigenvector and eigenvalue pair of $(\mathbf{G}+\mathbf{D})\bar{\mathbf{L}}$, then

$$(\mathbf{G}+\mathbf{D})\bar{\mathbf{L}}\boldsymbol{\upsilon} = \varphi\boldsymbol{\upsilon} \Leftrightarrow \bar{\mathbf{L}}\boldsymbol{\upsilon} = \varphi(\mathbf{G}+\mathbf{D})^{-1}\boldsymbol{\upsilon} \Rightarrow \frac{\boldsymbol{\upsilon}^T\bar{\mathbf{L}}\boldsymbol{\upsilon}}{\boldsymbol{\upsilon}^T(\mathbf{G}+\mathbf{D})^{-1}\boldsymbol{\upsilon}} = \varphi. \tag{29}$$

Since $\bar{\mathbf{L}}$ and $(\mathbf{G}+\mathbf{D})^{-1}$ are both positive definite

$$\boldsymbol{\upsilon}^T\bar{\mathbf{L}}\boldsymbol{\upsilon} > 0, \quad \boldsymbol{\upsilon}^T(\mathbf{G}+\mathbf{D})^{-1}\boldsymbol{\upsilon} > 0 \tag{30}$$

which results in $\varphi > 0$ and proves that $(\mathbf{G}+\mathbf{D})\bar{\mathbf{L}}$ is positive definite. For $\bar{\mathbf{L}}(\mathbf{G}+\mathbf{D})$ the result is the same.

Knowing that the cost function penalties are considered as positive definite, it can be concluded that $(\mathcal{B}^T\mathcal{Q}\mathcal{B})\succ 0$ and $(\mathbf{I}_\lambda\otimes\mathcal{W})\succ 0$ and therefore $\mathbf{S}$ is also positive definite. Note that constraints are disregarded in this case. ■

C. Distributed Algorithm

This cooperative approach is based on a distributed communication algorithm for 1-hop neighbors, resorting to the local optimization problem (13). At each instant of time, each agent f determines its solution and shares this same solution several times with its neighbors until it converges to an optimal control action sequence, of which only its first value is used. Then the algorithm is processed for the next instant of time. Consider $\hat{\mathbf{U}}_f(\gamma)$ as the estimate of $\mathbf{U}_f^*$ computed at iteration γ, as presented in Algorithm 1. In a practical implementation, a communications delay is considered as part of the model, and the time thus saved is used to transfer the data between vehicles.

Algorithm 1: 1-hop optimization algorithm for the agent $f\in\mathcal{N}$ at instant k

Input: tolerance $\sigma > 0$ and local error $\mathcal{E}_f$
Output: optimal control action sequence $\hat{\mathbf{U}}_f(\gamma)$

```
begin
    γ ← 0
    if (k = 0) then
        Û_f(0) ← random value
    else
        Û_f(0) ← U*_f(k − 1)
    end
    repeat
        broadcast Û_f(γ) to neighbors
        Û_f(γ + 1) ←
          argmin_{U_f} V_f (U_f; E_f, Û_{−f_1}(γ)) subject to
          the dynamics in (10)
        error ← ‖Û_f(γ + 1) − Û_f(γ)‖
        γ ← γ + 1
    until (error ≤ σ)
    return Û_f(γ)
end
```

At each iteration of the Algorithm 1, the following expression is satisfied

$$\mathbf{S}_f\hat{\mathbf{U}}_f(\gamma+1) - (g^f+d^f)(\mathcal{B}^T\mathcal{Q}\mathcal{B})\sum_{i\in\mathcal{N}_f}\hat{\mathbf{U}}_i(\gamma)+ \\ (g^f+d^f)(\mathcal{B}^T\mathcal{Q}\mathcal{A})\mathcal{E}_f - (g^f+d^f)^2(\mathcal{B}^T\mathcal{Q})\bar{\mathcal{E}}_d = \mathbf{0} \tag{31}$$

which can be expanded to include all the agents of the system

$$\left[(\mathbf{G}+\mathbf{D})^2\otimes(\mathcal{B}^T\mathcal{Q}\mathcal{B})+\mathbf{I}_\lambda\otimes\mathcal{W}\right]\hat{\mathbf{U}}(\gamma+1)- \\ \left[((\mathbf{G}+\mathbf{D})\mathbf{A}_d)\otimes(\mathcal{B}^T\mathcal{Q}\mathcal{B})\right]\hat{\mathbf{U}}(\gamma)+\left[(\mathbf{G}+\mathbf{D})\otimes(\mathcal{B}^T\mathcal{Q}\mathcal{A})\right]\mathcal{E} \\ -\left[(\mathbf{G}+\mathbf{D})^2\otimes(\mathcal{B}^T\mathcal{Q})\right](\bar{\mathcal{E}}_d)_{\times\lambda} = \mathbf{0}. \tag{32}$$

PROPOSITION 3. *Consider Algorithm 1 defined by the dynamics (32). Then, the local estimates of the optimal control $\hat{\boldsymbol{U}}$ converge to (25).*

Proof:
The expression (32) can be rewritten as a discrete system given by

$$\bar{\mathbf{A}}\bar{\mathbf{x}}(\gamma+1) - \bar{\mathbf{B}}\bar{\mathbf{x}}(\gamma) - \bar{\mathbf{c}} = \mathbf{0} \tag{33}$$

where $\bar{\mathbf{x}}, \bar{\mathbf{c}} \in \mathbb{R}^{n_0}$ and $\bar{\mathbf{A}}, \bar{\mathbf{B}} \in \mathbb{R}^{n_0\times n_0}$. Let $\boldsymbol{v}$ and φ be an arbitrary eigenvector and eigenvalue pair of $(\bar{\mathbf{A}}^{-1}\bar{\mathbf{B}})$, then

$$(\bar{\mathbf{A}}^{-1}\bar{\mathbf{B}})\boldsymbol{v} = \varphi\boldsymbol{v} \Leftrightarrow \\ \bar{\mathbf{B}}\boldsymbol{v} = \varphi\bar{\mathbf{A}}\boldsymbol{v} \Leftrightarrow \frac{\boldsymbol{v}^T\bar{\mathbf{B}}\boldsymbol{v}}{\boldsymbol{v}^T\bar{\mathbf{A}}\boldsymbol{v}} = \varphi \Rightarrow \frac{\boldsymbol{v}^T(\bar{\mathbf{B}}+\bar{\mathbf{B}}^T)\boldsymbol{v}}{\boldsymbol{v}^T 2\bar{\mathbf{A}}\boldsymbol{v}} = \varphi. \tag{34}$$

In order to have an asymptotically stable system, such that the state converges asymptotically to $\bar{\mathbf{x}}^* := (\bar{\mathbf{A}} - \bar{\mathbf{B}})^{-1}\bar{\mathbf{c}}$, it is necessary that $|\varphi|$ <1. Thus, from expression (34) it is possible to conclude that, for the system to be asymptotically stable, it is necessary that $\bar{\mathbf{A}} \succ 0$ and $2\bar{\mathbf{A}} \pm (\bar{\mathbf{B}} + \bar{\mathbf{B}}^T) \succ 0$.

Knowing that

$$\bar{\mathbf{A}} = \left[(\mathbf{G}+\mathbf{D})^2\otimes(\mathcal{B}^T\mathcal{Q}\mathcal{B})+\mathbf{I}_\lambda\otimes\mathcal{W}\right] \tag{35}$$

and

$$\bar{\mathbf{B}} = \left[((\mathbf{G}+\mathbf{D})\mathbf{A}_d)\otimes(\mathcal{B}^T\mathcal{Q}\mathcal{B})\right] \tag{36}$$

it can be concluded that $\bar{\mathbf{A}}$ is positive definite, since $(\mathbf{G}+\mathbf{D})^2 \succ 0$, $(\mathcal{B}^T\mathcal{Q}\mathcal{B}) \succ 0$ and $(\mathbf{I}_\lambda\otimes\mathcal{W}) \succ 0$. Regarding the second condition,

$$2\bar{\mathbf{A}} - (\bar{\mathbf{B}} + \bar{\mathbf{B}}^T) = \\ \left[\bar{\mathbf{L}}(\mathbf{G}+\mathbf{D}) + (\mathbf{G}+\mathbf{D})\bar{\mathbf{L}}\right]\otimes(\mathcal{B}^T\mathcal{Q}\mathcal{B}) \\ + 2\mathbf{I}_\lambda\otimes\mathcal{W} \succ 0 \tag{37}$$

and

$$2\bar{\mathbf{A}} + (\bar{\mathbf{B}} + \bar{\mathbf{B}}^T) = \\ [(\mathbf{G}+\mathbf{D}+\mathbf{A}_d)(\mathbf{G}+\mathbf{D}) + (\mathbf{G}+\mathbf{D})(\mathbf{G}+\mathbf{D}+\mathbf{A}_d)] \\ \otimes(\mathcal{B}^T\mathcal{Q}\mathcal{B}) + 2\mathbf{I}_\lambda\otimes\mathcal{W} \succ 0 \tag{38}$$

since, when defining an unsigned Laplacian matrix given by $\mathbf{L}_s = \mathbf{D} + \mathbf{A}_d$ which is positive semi-definite [26], it is possible to extrapolate that $(\mathbf{G}+\mathbf{D}+\mathbf{A}_d)(\mathbf{G}+\mathbf{D}) = (\mathbf{G}+\mathbf{L}_s)(\mathbf{G}+\mathbf{D}) \succ 0$ and $(\mathbf{G}+\mathbf{D})(\mathbf{G}+\mathbf{L}_s) \succ 0$. This proves that the system in (32) is asymptotically stable and converges to (25), if input and state constraints are not considered. The recursive feasibility and convergence of the optimization problem with further input and state constraints are left for future work. ■

D. Constraints

Although not considered in [18], constraints play a big part on the overall safety of the system, especially when dealing with multiple vehicles interacting with each other in their vicinities. With regard to the constraints $\mathcal{E}$considered in expression (13), control action constraints were included in order to restrict the fuel used by the thrusters, given by

$$\mathbf{u}_{min} \leq \mathbf{u}_f \leq \mathbf{u}_{max}. \tag{39}$$

Relative velocity constraints are also important for spacecraft proximity operations and passive security, in order to better react to emergencies, unforeseen scenarios that may happen or to prepare for docking,

$$(g^f+d^f)\mathbf{v}_{min} \leq \mathbf{v}_f \leq (g^f+d^f)\mathbf{v}_{max}. \tag{40}$$

Finally, minimum tracking error constraints were added for security and collision avoidance, given by

$$\|\mathcal{E}_f\|^2 \geq ((g^f+d^f)r_f)^2 \tag{41}$$

that is linearized around the point located at

$$\frac{(g^f+d^f)r_f}{\|\mathcal{E}_f\|}\mathbf{p}_f \tag{42}$$

and where r_f is the radius of the sphere representing the follower. This linearization is performed because the constraint (41) is non-convex.

IV. Simulation Results

This Section describes the simulation details and presents the results of the proposed control strategy for the three different communication scenarios presented in Fig. 2, followed by the discussion of these results. All simulations have been performed in MATLAB® R2019A with the help of the CasADi [27] library and the `solver(.)` method in order to get the optimal solution based on the current state, upper and lower bounds of the state and control constraints, initial and desired conditions. Simulating the same dynamics that were used to formulate the MPC proposed and disregarding the use of noise or sensors. To demonstrate the capabilities of the MPC that was formulated, a test scenario is simulated for each of the presented topologies, namely PLF, BDL and TPLF, and considering a system composed of four follower spacecrafts with the aim to achieve a V-bar station-keeping trajectory to each other at a constant relative position, like in a platoon scenario. Furthermore, it is considered that each spacecraft is close enough that the CW conditions are respected and the connection to the leader is maintain. The simulation parameters used to obtain these results are presented in Table I. In order to better illustrate the scenario that is being simulated here, an example is presented in Fig. 3 for the PLF topology.

The results for the three topologies considering four spacecrafts are presented in Fig. 4, 5, 6, 7, and 8. In these figures, besides validating that with any of the considered topologies the vehicles are able to achieve their objectives in the formation using a distributed framework, we can also see that vehicles that are at the tail of the formation have to adapt to the reactions of the other vehicles in the formation. This can be seen in the control effort variations that are more prominent in spacecrafts 3 and 4 relative to those of 1 and 2. Nonetheless, the convergence of their trajectories to the desired goals does is not visibly affected, as the time the relative velocities reach zero is almost the same.

Table II is composed by the RMSE (Root Mean Square Error), RMSEE (Root Mean Square of Energy Expended, in $\mathrm{m\,s^{-2}}$), and FOE (Final Output Error) parameters, which are respectively defined as

$$RMSE = \sqrt{\frac{1}{n_k}\sum_{k=0}^{n_k-1}\|\mathcal{E}(k)-\mathcal{E}_d(k)\|^2},$$

$$RMSEE = \sqrt{\frac{1}{n_k}\sum_{k=0}^{n_k-1}\|\mathbf{u}(k)\|^2},$$

$$FOE = \|\mathcal{E}(n_k)-\mathcal{E}_d(n_k)\|.$$

This table also supports the conclusion that all considered topologies yield overall convergence results of the same order of magnitude. Yet they provide further insight, as for most cases the best values are obtained for the PLF topology.

In all scenarios the proposed strategy manages to successfully converge the error to the desired values, while respecting the constraints that were imposed for each topology and with a behavior that goes according to the considered penalties. Since the four spacecraft were tested for the three network topologies, there is a disparity of behaviors that occurs in each situation depending on the number of agents connected to a given spacecraft and its distance from the leader. However, the goal was to have the same parameters for all topologies, since the objective is to complement the theoretical tests with a numerical validation of the proposed Algorithm.

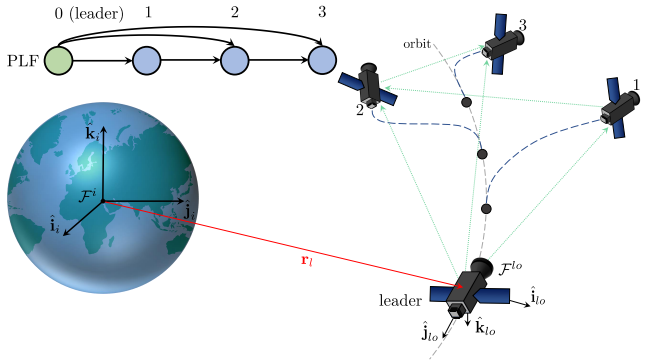

Fig. 3: Simulation illustration considering the PLF topology and 3 follower spacecraft

TABLE I: Simulation parameters of the DMPC for spacecraft platooning

Symbol	Value	Unit
μ	$3.986\,004\,41 \times 10^{14}$	$\mathrm{m^3\,s^{-2}}$
$\|^i\mathbf{r}_l\|$	6621000	m
$\mathbf{p}_1(0)$	$\begin{bmatrix}30 & -35 & 40\end{bmatrix}^T$	m
$\mathbf{p}_2(0)$	$\begin{bmatrix}15 & -46 & -30\end{bmatrix}^T$	m
$\mathbf{p}_3(0)$	$\begin{bmatrix}-49 & -43 & -20\end{bmatrix}^T$	m
$\mathbf{p}_4(0)$	$\begin{bmatrix}-29 & -23 & 37\end{bmatrix}^T$	m
$\mathbf{v}_f(0)$	$\begin{bmatrix}0 & 0 & 0\end{bmatrix}^T$	$\mathrm{m\,s^{-1}}$
$\mathcal{E}_d$	$\begin{bmatrix}0 & -8 & 0 & 0 & 0 & 0\end{bmatrix}^T$	
T_s	0.1	s
n_k	180	
N	30	
$\mathbf{P}$	$25\mathbf{I}_6$	
$\mathbf{Q}$	$13\mathbf{I}_6$	
$\mathbf{W}$	$0.1\mathbf{I}_3$	
σ	0.5	
$[\alpha_1\ \alpha_2\ \alpha_3\ \alpha_4]$	$\begin{bmatrix}2 & 1.5 & 1 & 1\end{bmatrix}$	
$\mathbf{u}_{max}$	6	$\mathrm{m\,s^{-2}}$
$\mathbf{v}_{max}$	20	$\mathrm{m\,s^{-1}}$
r_f	3	m

TABLE II: Simulation performance of the DMPC for spacecraft platooning

f	Network	RMSE	RMSEE	FOE
1	PLF	**19.781**	4.930	$\mathbf{3.262 \times 10^{-6}}$
	BDL	41.506	**4.697**	7.180×10^{-6}
	TPLF	19.980	5.064	3.783×10^{-6}
2	PLF	36.932	4.807	$4.873e \times 10^{-6}$
	BDL	44.486	**4.682**	5.385×10^{-6}
	TPLF	**36.829**	4.840	$\mathbf{4.727 \times 10^{-6}}$
3	PLF	**40.557**	4.884	$\mathbf{6.726 \times 10^{-6}}$
	BDL	50.787	**4.346**	1.035×10^{-5}
	TPLF	71.448	4.665	1.419×10^{-5}
4	PLF	**31.953**	**3.985**	$\mathbf{4.670 \times 10^{-6}}$
	BDL	33.542	4.836	7.941×10^{-6}
	TPLF	58.155	4.214	8.990×10^{-6}

The linearized version of the minimum tracking error constraint is also satisfied, as seen in Fig. 8.

Analyzing the individual results of the follower 1 in the different network topologies, presented in Fig. 4, it can be concluded that the error position continuously converges without oscillation to the desired value. This desired value and initial condition will vary for each topology, since it depends on the number of neighbors to which it is connected, explaining the difference between the BDL topology and the others. The same can be said for the error velocity where there is an absolute increase in the initial velocity until it reaches a peak maximum, and then converges to zero, with a significant difference in slopes depending on the topology. Comparing the PLF and TPLF for follower 1, which present the same initial conditions and the same desired value, it can be concluded that the PLF has slightly superior results, especially when observing the control action and results of Table II. It is, however, a minor difference of performance.

For the follower 2, the results presented in Fig. 5, show that the PLF and TPLF topologies have very similar

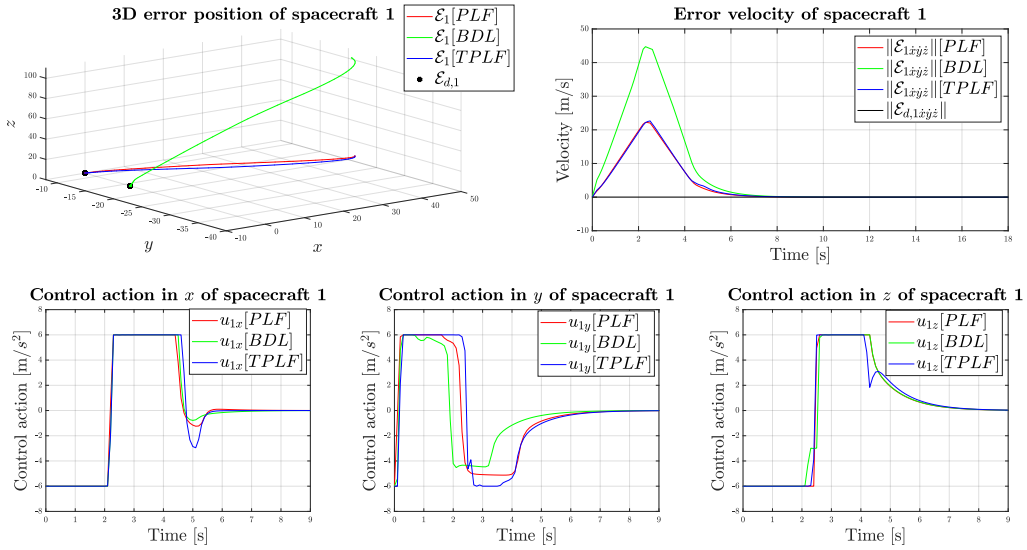

Fig. 4: Simulation results of the DMPC for spacecraft platoon (Follower 1)

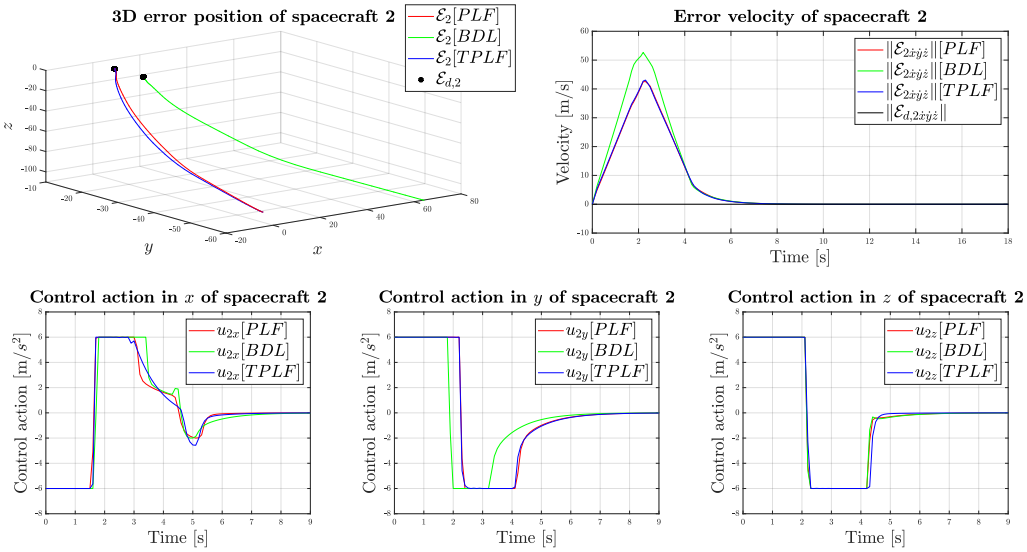

Fig. 5: Simulation results of the DMPC for spacecraft platoon (Follower 2)

behaviors, the most significant difference being in the control action at x where the PLF topology shows more oscillation. From Table II it can also be concluded that the PLF has sightly worst results than TPLF.

Moving on to the results of follower 3, presented in Fig. 6, it is already possible to observe three different trajectories for each of the topologies, highlighting the overshoot in the z error position for the PLF topology. In the control action, the BDL presents significantly more oscillation than the other topologies.

Finally, for the results of follower 4, presented in Fig. 7, it can be observed that, despite the PLF and BDL topologies having the same initial condition and the same desired position, they follow different trajectories. Of these two topologies, the PLF is faster and with less overshoot. This comparison is also seen in Table II, where PLF performs better on all criteria. Supporting the idea that the PLF topology is better suited for this specific situation under this parameters.

In summary, the presented results validate the proposed methodology for several scenarios involving different network topologies, considering multiple spacecraft and accounting for input and state constraints. We can also see that the farther a spacecraft is from the leader, a greater degradation of performance is present in the system response, more visible for Follower 4. It can also be seen that the TPLF has in general better performance in the transient networks response.

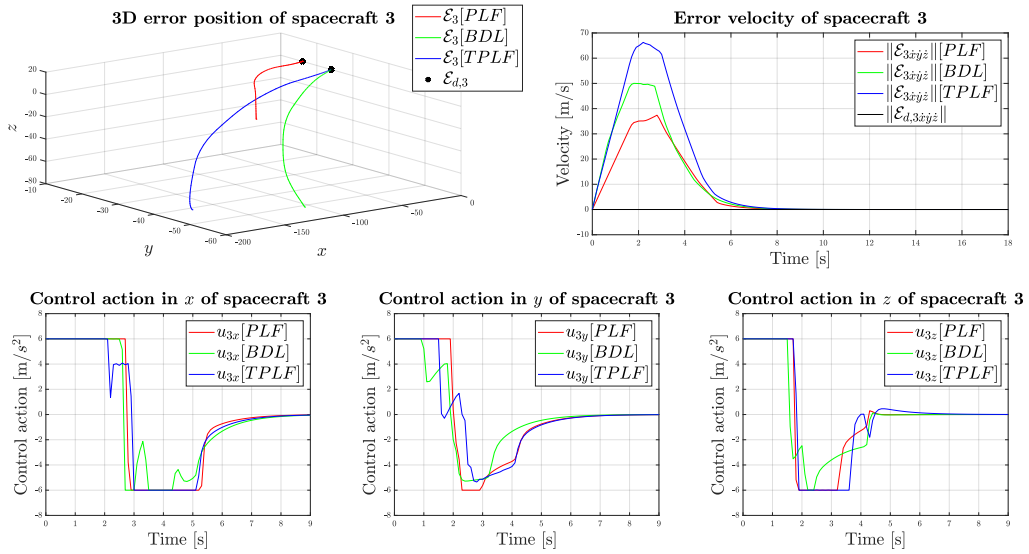

Fig. 6: Simulation results of the DMPC for spacecraft platoon (Follower 3)

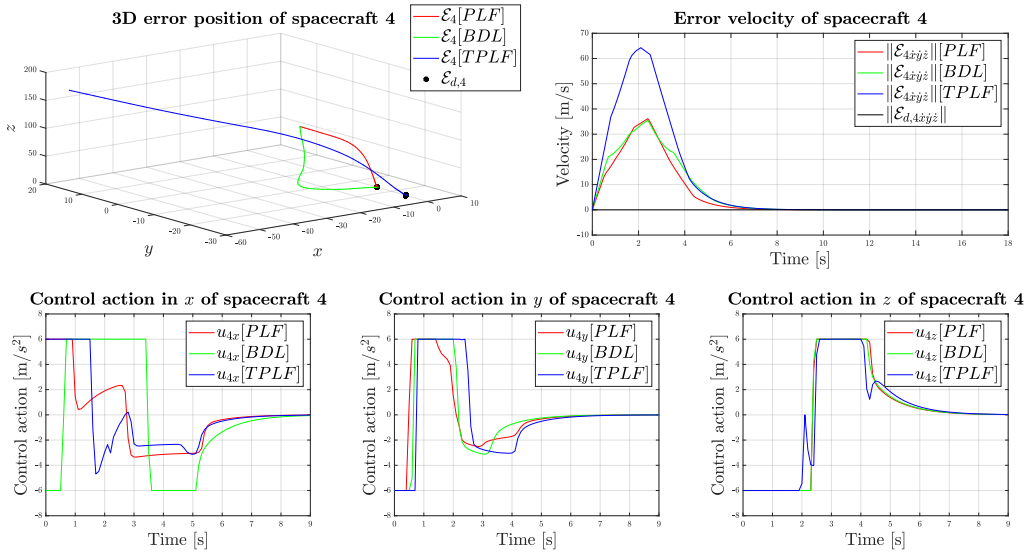

Fig. 7: Simulation results of the DMPC for spacecraft platoon (Follower 4)

V. Conclusion

The goal of this paper was to design and rethink the spacecraft formation flying problem, in a more cooperative and optimal solution for the spacecraft synchronization scenario. It was considered for that a distributed platooning algorithm that solves an 1-hop optimization problem with relevant constraints in order to generate better and safer trajectories for station-keeping trajectories. In a second stage, the proposed strategy was validated through simulated tests in MATLAB®, where different maneuvers are efficiently performed while satisfying all the constraints considered.

It was also showed that each optimization problem is solved within a sampling period, which includes the vehicle model constraint, has a unique feasible solution, and that solving the distributed optimization problem at each agent, considering the 1-hop distributed algorithm, converges to the global centralized solution. Adding further input and state constraints, if not carefully validate, can obviously disrupt the feasibility of the optimization problem. On the other hand, feasibility at each sampling period may not be enough to ensure a sufficient decrease of the cost functional between sampling periods when working outside nominal conditions. Therefore, there are techniques that can be considered to address both the addition of constraints and the recursive feasibility, which are considered outside the scope of the paper and left for future work. Besides that, there are some work directions

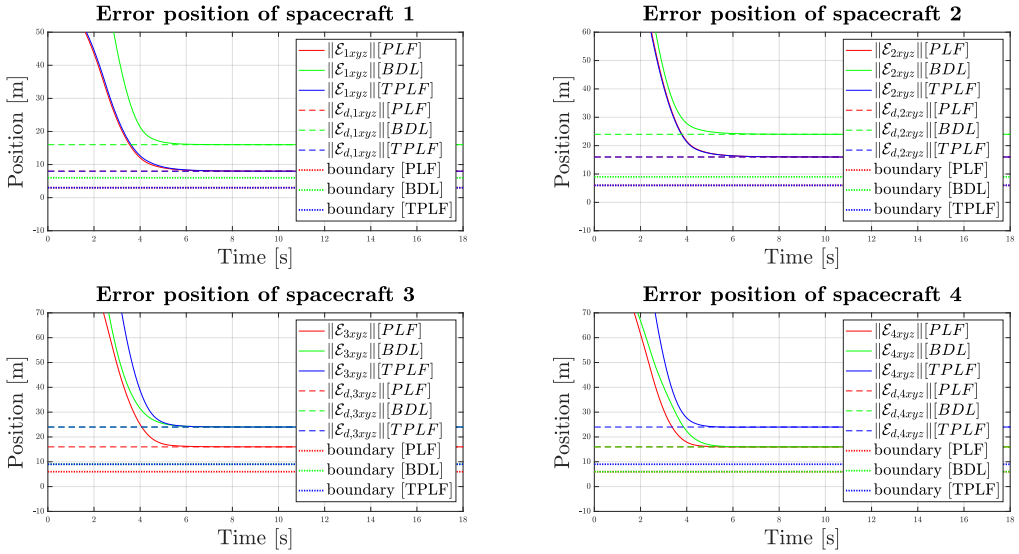

Fig. 8: Simulation results of the DMPC for spacecraft platoon considering the minimum tracking error constraint

that can be pursued, for example a relative rotational motion could be added in order to control the spacecraft attitude and more network topologies could be considered and analyzed.

REFERENCES

[1] D. C. Woffinden and D. K. Geller
Navigating the road to autonomous orbital rendezvous
Journal Spacecraft Rockets, vol. 44, no. 4, p. 898–909, 2007.

[2] Q. Li, J. Yuan, B. Zhang, and C. Gao
Model predictive control for autonomous rendezvous and docking with a tumbling target
Aerospace Science and Technology, vol. 69, pp. 700–711, 2017.

[3] S. Kimura, E. Atarashi, T. Kashiwayanagi, K. Fujimoto, and R. Proffitt
Low-cost and high-performance visual guidance and navigation system for space debris removal
Advanced Robotics, vol. 35, no. 21-22, pp. 1277–1285, 2021.

[4] S.-I. Nishida, S. Kawamoto, Y. Okawa, F. Terui, and S. Kitamura
Space debris removal system using a small satellite
Acta Astronautica, vol. 65, no. 1, pp. 95–102, 2009.

[5] J. R. Wertz and W. J. Larson
Space Mission Analysis and Design. Torrance, USA: Microcosm Press, 1999.

[6] J. B. Rawlings and D. Q. Mayne
Model Predictive Control: Theory and Design. Madison, Wisconsin: Nob Hill Publishing, 2009.

[7] J. C. Sanchez, F. Gavilan, and R. Vazquez
Chance-constrained model predictive control for near rectilinear halo orbit spacecraft rendezvous
Aerospace Science and Technology, vol. 100, p. 105827, 2020.

[8] L. Ravikumar, R. Padhi, and N. Philip
Trajectory optimization for rendezvous and docking using nonlinear model predictive control
IFAC-PapersOnLine, vol. 53, no. 1, pp. 518–523, 2020.

[9] A. K. Larsén *et al.*
A computationally efficient model predictive control scheme for space debris rendezvous
IFAC-PapersOnLine, vol. 52, no. 12, pp. 103–110, 2019.

[10] R. Chai, A. Tsourdos, H. Gao, Y. Xia, and S. Chai
Dual-loop tube-based robust model predictive attitude tracking control for spacecraft with system constraints and additive disturbances
IEEE Transactions on Industrial Electronics, vol. 69, no. 4, pp. 4022–4033, 2022.

[11] R. Chai, A. Tsourdos, H. Gao, S. Chai, and Y. Xia
Attitude tracking control for reentry vehicles using centralised robust model predictive control
Automatica, vol. 145, p. 110561, 2022.

[12] W. Wang, C. Li, and Y. Guo
Relative position coordinated control for spacecraft formation flying with obstacle/collision avoidance
Nonlinear Dynamics, vol. 104, no. 2, pp. 1329–1342, 2021.

[13] J. Scharnagl, P. Kremmydas, and K. Schilling
Model predictive control for continuous low thrust satellite formation flying
IFAC-PapersOnLine, vol. 51, no. 12, pp. 12–17, 2018.

[14] J. Scharnagl, F. Kempf, and K. Schilling
Combining distributed consensus with robust H_∞-control for satellite formation flying
Electronics, vol. 8, no. 319, 2019.

[15] Y. Zheng, S. E. Li, K. Li, F. Borrelli, and J. K. Hedrick
Distributed model predictive control for heterogeneous vehicle platoons under unidirectional topologies
IEEE Transactions on Control Systems Technology, vol. 25, no. 3, pp. 899–910, 2017.

[16] R. Olfati-Saber and R. Murray
Consensus problems in networks of agents with switching topology and time-delays
IEEE Transactions on Automatic Control, vol. 49, no. 9, pp. 1520–1533, 2004.

[17] W. Ren and R. Beard
Consensus seeking in multiagent systems under dynamically changing interaction topologies
IEEE Transactions on Automatic Control, vol. 50, no. 5, pp. 655–661, 2005.

[18] H. Ferraz and J. Hespanha
Iterative algorithms for distributed leader-follower model predictive control
In *2019 IEEE 58th Conference on Decision and Control (CDC)*, 2019, pp. 3533–3539.

[19] S. Mansouri, G. Nikolakopoulos, and T. Gustafsson

Distributed model predictive control for unmanned aerial vehicles
In *2015 Workshop on Research, Education and Development of Unmanned Aerial Systems (RED-UAS)*, 2015, pp. 152–161.

[20] N. Esfahani and K. Khorasani
A distributed model predictive control (MPC) fault reconfiguration strategy for formation flying satellites
International Journal of Control, vol. 89, no. 5, pp. 960–983, 2016.

[21] P. Pereira, B. Guerreiro, and P. Lourenço
Cooperative platooning and servicing for spacecraft formation flying using model predictive control
In *CEAS EuroGNC 2022 – Conference on Guidance, Navigation and Control*, May 2022.

[22] W. Fehse
Automated Rendezvous and Docking of Spacecraft. Cambridge, UK: Cambridge University Press, 2003.

[23] W. Clohessy and R. Wiltshire
Terminal guidance system for satellite rendezvous
Journal of Aerospace Sciences, vol. 27, no. 9, p. 653–658, 1960.

[24] N. G. Ortolano
Autonomous trajectory planning for satellite RPO and safety of flight using convex optimization
Ph.D. dissertation, Aerospace Engineering, Utah State University, Utah, USA, 2018. [Online]. Available: https://digitalcommons.usu.edu/etd/7291/

[25] E. N. Hartley
A tutorial on model predictive control for spacecraft rendezvous
In *2015 European Control Conference (ECC)*, 2015, pp. 1355–1361.

[26] S. Kirkland and D. Paul
Bipartite subgraphs and the signless Laplacian matrix
Applicable Analysis and Discrete Mathematics, vol. 5, no. 1, pp. 1–13, 2011.

[27] J. A. E. Andersson, J. Gillis, G. Horn, J. B. Rawlings, and M. Diehl
CasADi – A software framework for nonlinear optimization and optimal control
Mathematical Programming Computation, vol. 11, no. 1, pp. 1–36, 2019.

Pedro Pereira received the B.Sc. and M.Sc. degrees in Electrical and Computer Engineering in 2019 and 2021, respectively, from NOVA School of Science and Technology (FCT-NOVA), Lisbon, Portugal. He was awarded the Talkdesk Merit Award for his Master's dissertation on Model Predictive Control Applications for the Cooperative Rendezvous of Satellites as well as the Best Student Award for his M.Sc. degree.

Since 2022, he has been an Autonomous Driving Software Engineer at Critical TechWorks, from the BMW Group, with past experiences at Siemens, NTT Data, KPMG, and Volkswagen Digital Solutions focusing on software development. His current research interests include spacecraft control systems, embedded systems, computer vision algorithms, and autonomous driving solutions, mainly for lateral features and hands off driving.

Bruno Guerreiro (Member, IEEE) received the Licenciatura and Ph.D. degrees in Electrical and Computer Engineering in 2004 and 2013, respectively, both from Instituto Superior Técnico (IST), Lisbon, Portugal, and his Ph.D. thesis received the Best Ph.D. Thesis Award by the Portuguese Robotics Society. He is currently an Assistant Professor with the NOVA School of Science and Technology and CTS/UNINOVA, Universidade Nova de Lisboa (FCT/UNL), and a researcher with the Institute for Systems and Robotics (ISR-Lisboa, LARSYS), at Instituto Superior Técnico, Lisbon, Portugal. His scientific activity has focused on theoretical, practical, and technological challenges related to the use of aerospace robotics for civilian applications, while his research interest include sensor-based SLAM, trajectory planning, linear and nonlinear control, model predictive control, automatic LIDAR calibration, and modeling of aerial and marine vehicles.

Pedro Lourenço received the BSc and MSc degrees in Aerospace Engineering in 2010 and 2012, respectively, both from Instituto Superior Técnico (IST), Lisbon, Portugal, on the course of which he received the Merit Award. In 2019, he then received his Ph.D. degree in Electrical and Computer Engineering from IST, while being a researcher with the Institute for Systems and Robotics. He was awarded the Best National Ph.D. Thesis in Robotics by the Portuguese Robotics Society for his dissertation on globally convergent simultaneous localization and mapping.

In 2019, he joined the GNC division of the Flight Segment and Robotics business unit of GMV, Lisbon, Portugal as a control specialist designing GNC/AOCS systems for spacecraft in ESA-contracted activities. Since 2022, he became Head of Guidance & Control Section and has lead R&D&I efforts towards the adoption of optimization-based guidance & control, with emphasis on the enhancement of the verification and validation process and robustification of algorithms. His research interests include optimization-based guidance & control, model predictive control, active estimation, with particular emphasis on spacecraft AOCS/GNC.